Lattice-Boltzmann Method For Fast Patient-Specific Simulation of Liver Tumor Ablation from CT Images

Chloé Audigier, Tommaso Mansi, Hervé Delingette, Saikiran Rapaka, Viorel Mihalef, Puneet Sharma, Ali Kamen, Daniel Carnegie, Emad Boctor, Michael Choti, et al.

▶ **To cite this version:**

Chloé Audigier, Tommaso Mansi, Hervé Delingette, Saikiran Rapaka, Viorel Mihalef, et al.. Lattice-Boltzmann Method For Fast Patient-Specific Simulation of Liver Tumor Ablation from CT Images. Proceedings of Medical Image Computing and Computer Assisted Intervention 2013 (MICCAI), Sep 2013, Nagoya, Japan. hal-00804147v1

HAL Id: hal-00804147

https://inria.hal.science/hal-00804147v1

Submitted on 25 Mar 2013 (v1), last revised 17 Jul 2013 (v2)

HAL is a multi-disciplinary open access archive for the deposit and dissemination of scientific research documents, whether they are published or not. The documents may come from teaching and research institutions in France or abroad, or from public or private research centers.

L'archive ouverte pluridisciplinaire **HAL**, est destinée au dépôt et à la diffusion de documents scientifiques de niveau recherche, publiés ou non, émanant des établissements d'enseignement et de recherche français ou étrangers, des laboratoires publics ou privés.

Lattice-Boltzmann Method For Fast Patient-Specific Simulation of Liver Tumor Ablation from CT Images

C Audigier[1,2], T Mansi[2], H Delingette[1], S Rapaka[2], V Mihalef[2], P Sharma[2], A Kamen[2], D Carnegie[4], E Boctor[3], M Choti[4], D Comaniciu[2], N Ayache[1]

[1] INRIA Sophia-Antipolis, Asclepios Research Group, Sophia-Antipolis, France
[2] Siemens Corporate Research, Imaging and Computer Vision, Princeton, NJ, USA
[3] Dept. of Radiology, Johns Hopkins Medical Institutions, Baltimore, Maryland, USA
[4] Dept. of Surgery, Johns Hopkins Medical Institutions, Baltimore, Maryland, USA

Abstract. Radio-frequency ablation (RFA), the most widely used minimally invasive ablative therapy of liver cancer, is challenged by a lack of patient-specific planning. In particular, the presence of blood vessels and time-varying thermal diffusivity makes the prediction of the extent of ablated tissue difficult. This may result in incomplete treatments and increased risk of recurrence. In this manuscript, we propose a new model of the biological mechanisms involved in RFA of abdominal tumors based on Lattice Boltzmann Method (LBM) to predict the extent of ablation given probe location and biological parameters. Our method relies on patient images, from which a level set representation of liver geometry, tumor shape and vessels is extracted. Then, a computational model of heat diffusion, cellular necrosis and blood flow through vessels and liver is solved to estimate the extent of ablated tissue. After quantitative verifications against an analytical solution, we apply our framework on three patients for whom pre- and post-operative CT data were available, yielding promising correlation (point to mesh errors of 4.3 $\pm$ 2.7, 6.0$\pm$ 3.6 and 11.9 $\pm$ 5.2 mm with ground truth). Implemented on graphics processing units, our method enables for the first time real-time computation: seven minutes of ablation are simulated in eight minutes, which is $\approx 60\times$ faster than standard finite element methods. Our approach may thus enable model-based planning of RFA in clinical settings.

1 Introduction

In spite of recent advances in cancer therapy, treatment of primary and metastatic tumors of the abdomen, including the liver, remains a significant challenge. Hepatocellular carcinoma (HCC) for example is one of the most common malignancies encountered throughout the world (more than 1 million cases per year), with increasing frequency in Western countries due to the changing prevalence of hepatitis C [1]. Unfortunately, less than 25% of patients with primary or secondary liver cancer are candidates for resection or transplantation, the most effective treatments. Consequently, ablative therapies such as radiofrequency ablation (RFA) has raised increasing interest for the treatment of liver tumors.

RFA procedure consists in placing a probe within the target area in the liver parenchyma. Electrodes at the tip of the probe create heat, which is conducted

into the surrounding tissue, causing coagulative necrosis at temperatures above 50°C. Success of the procedure depends on the optimal placement of the probe and heat delivery. However, this task is challenged by the hepatic blood vessels that dissipate heat, thus potentially reducing RFA efficiency and increasing risks of recurrence.

Several studies [2–4] have investigated finite-element methods (FEM) to compute heat diffusion in liver and predict the optimal placement of the RFA probes. Heat sink models have been studied, as well as various cellular necrosis models [5]. However, to the best of our knowledge, none of these models rely on patient-specific data. In particular, the vascular system of the liver is neglected or simplified and blood flow circulation is not computed based on patient-specific clinical information. Moreover, FEM method are computationally demanding, with execution time in the range of hours, which is not suitable for clinical purposes nor therapy guidance.

This paper presents a multi-physics model for efficient patient-specific planning of RFA based on medical images such as CT or MRI (Sec. 2). In particular, we rely on Lattice-Boltzmann method (LBM) to compute heat diffusion in the liver tissue. LBM offer high parallel scalability, second order accuracy in space and the simplicity of implementation on a uniform Cartesian grid [6]. Owing to these appealing properties, LBM has emerged as a powerful technique for efficient simulation of a large class of partial-differential equations [7]. In Sec. 3, we demonstrate the validity of our algorithm against an analytical solution and we evaluate its predictive power on patient data. Sec. 4 concludes the manuscript.

2 Method

Fig. 1 illustrates the different steps of our method. Starting from a preoperative clinical CT image, we extract the liver geometry and the venous system. Next, we solve the bioheat equation using LBM. To cope with the different blood compartments, we combine different bioheat models: the Pennes model [8] close to the larger vessels and the Wulff and Klinger model [9] elsewhere to consider the effect of smaller vessels on heat diffusion. The bioheat equation is coupled to a computational fluid dynamics (CFD) solver to accurately take into account the effect of blood circulation on the dissipated heat, while the blood flow in the porous tissue is computed by solving the Darcy's equation. LBM and CFD are calculated on a Cartesian grid while the porous solver is executed on a tetrahedral mesh for increased accuracy. Finally, a cellular necrosis model is employed to compute cell death due to over-heating [5].

2.1 Anatomical Model

Preoperative images (CT, MRI) are semi-automatically segmented, yielding a detailed anatomical model of patient's liver, including parenchyma, tumors, hepatic veins, vena cava, portal vein and the hepatic artery if visible (Fig. 2, left panel). For each structure, the user defines seeds inside and outside the area of interest. Then, the random-walker algorithm is employed [10] to automatically estimate the boundaries of the structure. The process can be refined by the user,

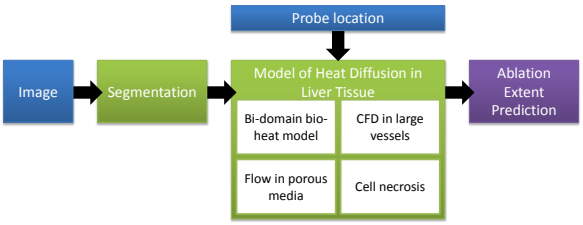

Fig. 1. Main steps of the proposed method (blue: input data, green: processes, purple: output). *See text for details.*

interactively. From the segmentation, a level set representation of the liver, minus tumor and vessels is calculated. A multi-label mask image is also created to identify the structures of interest for the simulation. Finally, a tetrahedral multi-domain mesh is generated automatically based on the resulting segmentations (www.cgal.org) for calculating the porous flow.

2.2 Model of Heat Transfer in Liver Tissue

Computing heat diffusion in biological tissues amounts to solving the coupled bioheat equations derived from the theory of porous media, where each elementary volume is assumed to comprise fraction of tissue and blood [11]. Because current imaging techniques do not allow to estimate the accurate ratio between blood and liver tissue, two main simplifications of the bioheat equations have been proposed. The *Pennes model* [8] assumes constant blood temperature, which holds close to large vessels, where blood velocity is high. The model writes: $(1-\epsilon)\rho_t c_t \partial T/\partial t = (1-\epsilon)Q + (1-\epsilon)\nabla.(d_t \nabla T) + H(T_{b0} - T)$. Reversely, The *Wulff-Klinger (WK) model* [9] assumes equilibrium between tissue and blood temperatures, with a blood volume fraction $\epsilon \ll 1$. This model, which is well-suited for small vessels where blood velocity is low, writes: $(1-\epsilon)\rho_t c_t \partial T/\partial t = (1-\epsilon)Q + (1-\epsilon)\nabla.(d_t \nabla T) - \epsilon \rho_b c_b \mathbf{v}.\nabla T$. In both equations, T, Q, $\mathbf{v}$ and T_{b0} stand for temperature, source term, blood velocity and the mean temperature (assumed constant) of the blood in large vessels. The other parameters are summarized in Table 1. In our framework, we use either the Pennes model or the WK model according to the spatial location in the liver anatomy. Assuming that blood vessels and surrounding tissue are isolated from each other, we compute the temperature T by solving the diffusion equation $\rho_t c_t \partial T/\partial t = Q + \nabla.(d_t \nabla T)$ everywhere in the domain, to which we add the cooling term $H(T_{b0} - T)/(1-\epsilon)$ when a point belongs to a large vessel (Pennes model) or $-\epsilon \rho_b c_b \mathbf{v}.\nabla T/(1-\epsilon)$ when it belongs to the parenchyma (WK model).

2.3 Model of the Hepatic Venous Circulation System

Blood velocity $\boldsymbol{v}$ inside the parenchyma is calculated according to Darcy's law $\boldsymbol{v} = -\kappa/(\mu\epsilon^{2/3})\nabla p$, where p is the pressure. This amounts to solving the Laplace equation $\nabla \cdot (-\kappa/(\mu\epsilon^{2/3})\nabla p) = 0$. At the border of the liver, Neumann boundary conditions are employed whereas at the tip of the portal and hepatic veins,

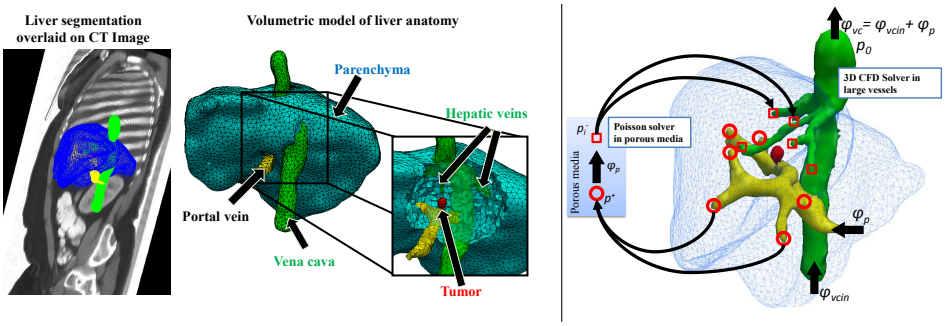

Fig. 2. *Left*: A detailed anatomical model of the liver is estimated from standard clinical CT image. *Right*: Model of the hepatic circulatory system. Arrows denote blood flow. Circles and squares denote portal and hepatic vessel tips. *See text for details.*

Dirichlet boundary conditions are applied to define the pressure drop between the veins. Since we cannot estimate these pressures in-vivo, we rely on a CFD model of the hepatic venous circulation system to estimate them (Fig. 2). Let $\varphi_{vc_{in}}$ be the vena cava inflow, φ_p the portal vein inflow, $\varphi_{vc} = \varphi_{vc_{in}} + \varphi_p$ the vena cava outflow (conservation of mass, the hepatic artery is neglected in this first embodiment but could be added without modification into the framework) and φ_i the flow through the inlets of the hepatic veins. We also assume the vena cava outlet pressure $p_0 = 3\,mmHg$, in the range of physiological values of healthy patients. First, we compute the blood flow and pressure distribution within the vena cava and hepatic veins (Fig. 2) using 3D CFD (unsteady incompressible Navier-Stokes equations with viscous terms). The blood is modeled as a Newtonian fluid with pre-specified density ρ_b and viscosity μ (Table 1). A plug profile velocity field is applied at the inlets (squares in Fig. 2), computed from the outflow φ_p and the cross-sectional area of each inlet. From the CFD computation we get the downstream pressures p_i^- for each inlet of the hepatic vein. We then estimate the upstream pressure p^+, assumed constant, of the portal vein outlets (circles in Fig. 2). To that end, we solve the Darcy's law and optimize over p^+ such that the computed perfused flow through the hepatic vein inlets matches the one computed using 3D CFD. Once p^+ is estimated, we compute the blood flow inside the portal vein using the 3D CFD solver. In this work, the effect of heat on the viscosity of the flow is neglected to decouple flow-related computation from heat diffusion calculation for computational efficiency.

2.4 Model of cellular necrosis

Tissue necrosis is computed based on the simulated temperatures using a three-state model [5]. The model computes the variation of concentration of alive (A), vulnerable (V) and dead (D) cells over time according to the state equation: $\mathrm{A} \underset{k_b}{\overset{k_f(T)}{\rightleftarrows}} \mathrm{V} \xrightarrow{k_f(T)} \mathrm{D}$ where $k_f(T) = \bar{k_f} e^{T/T_k}(1-A)$ and k_b are the rates of cell damage and recovery respectively. $\bar{k_f}$ is a scaling constant and T_k a parameter

that sets the rate of the exponential increase with temperature. This equation results in three coupled ODEs that we solve with a first order explicit scheme at each vertex of the Cartesian grid, yielding a spatially-varying cell state field then used in the bioheat solver. The initial condition are chosen as in [5]. During the computation of heat diffusion, the heat capacity is updated according to the state of the cell: c_t for alive or damaged cells, c_t^* for dead cells.

2.5 Lattice-Boltzmann Formulation of the Bioheat Equations

The bioheat model is solved on an isotropic Cartesian grid using LBM with 7-connectivity topology and Neumann boundary conditions. The governing equation at position $\mathbf{p} = (x, y, z)$ for the edge $\mathbf{e}_i$ is given by $\mathbf{f}(\mathbf{p} + \mathbf{e_i}\Delta p, t + \Delta t) = \mathbf{f}(\mathbf{p}, t) + \mathbf{A}[\mathbf{f}^{eq}(\mathbf{p}, t) - \mathbf{f}(\mathbf{p}, t)] + \boldsymbol{\omega}\Delta t H(T_{b0} - T(\mathbf{p}, t))$, where $c = \frac{\Delta p}{\Delta t}$, $c_s^2 = 1/4$, Δp is the spacing and $f_i^{eq}(\mathbf{p}, t) = \omega_i T(\mathbf{p}, t)[1 + \frac{\mathbf{e_i}.\mathbf{v}}{cc_s^2}]$. $\mathbf{f}(\mathbf{p}) = \{f_i(\mathbf{p})\}_{i=1..7}$ is the vector of distribution function with $f_i(\mathbf{p})$, the probability of finding a particle travelling along the edge $\mathbf{e}_i$ of the node $\mathbf{p}$ at a given time, and $\boldsymbol{\omega} = \{\omega_i\}_{i=1..7}$ the vector of weighting factors [6]. The temperature is computed as $T(\mathbf{p}, t) = \sum_{i=1}^{7} f_i(\mathbf{p}, t)$ and is updated at every node of the grid for every timestep. By the mean of the level set representation, the boundaries can be treated differently using linear interpolation without requiring advanced meshing techniques [12]. For a matter of stability, we use a Multiple-Relaxation-Time model, the collision matrix $\mathbf{A}$ is written as $\mathbf{M^{-1}SM}$, where $\mathbf{M} = \begin{pmatrix} 1 & 1 & 1 & 1 & 1 & 1 & 1 \\ 0 & 1 & -1 & 0 & 0 & 0 & 0 \\ 0 & 0 & 0 & 1 & -1 & 0 & 0 \\ 0 & 0 & 0 & 0 & 0 & 1 & -1 \\ 6 & -1 & -1 & -1 & -1 & -1 & -1 \\ 0 & 2 & 2 & -1 & -1 & -1 & -1 \\ 0 & 0 & 0 & 1 & 1 & -1 & -1 \end{pmatrix}$ and $\mathbf{S} = \mathrm{diag}(1, 1/\tau, 1/\tau, 1/\tau, 0.7519, 0.7519, 0.7519)$. The relaxation time τ is directly related to the diffusion coefficient D through $\tau = 1/2 + 4D\Delta t/\Delta p^2$. Finally, we model the heat source term through a Dirichlet boundary condition at the location of the probe. For the CFD computation, we use a full 3D Navier-Stokes viscous solver, expressed in an Eulerian framework which embeds the domain boundary using a level set representation of the segmented vessels [13]. The porous flow is calculated using FEM on the linear multi-domain tetrahedral mesh. The resulting flow is tri-linearly rasterized on the Cartesian grid after computation. CFD and porous flow are calculated only once, at the beginning of the algorithm.

3 Experiments and Results

3.1 Quantitative Verification Against Analytical Solution

To evaluate our model, we compared its behavior on a regular cuboid domain with the 3D analytical solution of a source of mass M released at location $\boldsymbol{p_0}$ at time t_0 of the advection-diffusion equation $\partial T/\partial t + \mathbf{v}.\nabla T = \nabla(D\nabla T)$:

$$T(\boldsymbol{p}, t) = \frac{M}{[4\pi(t - t_0)D]^{3/2}} \exp\left(-\frac{\|\boldsymbol{p} - \boldsymbol{p_0} - (t - t_0)\boldsymbol{v}\|^2}{4D(t - t_0)}\right)$$

Parameters were chosen to get heat diffusion in physiological range: $D = 0.1\,mm^2/s$, $\boldsymbol{v} = (2, 0, 0)\,mm/s$, $M = 35000\,°\mathrm{C}/mm^3$, $t_0 = -50\,s$, yielding a Gaussian-shape source term of 70 °C at the center at time $t = 0\,s$. In our LBM solver, we initialized the temperature values at each point with the analytical solution at time $t = 0\,s$. The temperature at several points of the domain was reported. Our implementation was qualitatively close to the analytical solution (Fig. 3). For a given resolution, an upper and lower bound for the time-step were provided by the simulated physics and the Courant-Friedrichs-Lewy conditions. As expected, the smaller the spatial resolution, the more accurate our solution. A time-step of $75\,ms$ and a resolution of $1 - 2\,mm$ appeared to be a good compromise between accuracy and computational cost. All experiments were executed on a Windows 7 desktop machine (Intel Xeon, 2.80 Hz, 45GB RAM) with a Nvidia Quadro 6000 1.7 GB. From a computational point of view, experiments showed a speed-up of 11 with parallel optimization (OpenMP) and 45 with graphical processing units (GPU) implementation on CUDA with respect to single-core implementation of LBM. Non-reported experiments showed that 60× speed-up was obtained with respect to FEM for similar accuracy.

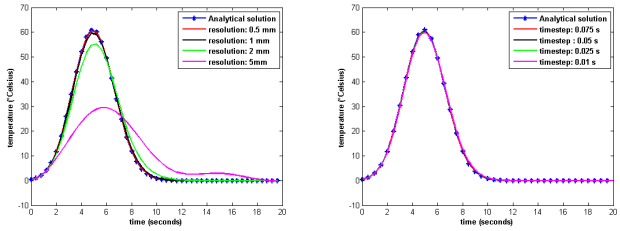

Fig. 3. *Left*: Spatial convergence analysis for a fixed time-step of 0.01 s. *Right*: Time convergence analysis for a resolution of 1 mm compared to the analytical solution. As one can see, the proposed framework quickly converges to the right solution.

3.2 Evaluation on Patient Data

We evaluated our model on three patients for whom preoperative CT images and postoperative CT images (patient 1 and 3) and MR images (patient 2) were available. For all patients, nominal tissue parameters were employed. Clinical RFA protocol was as follows. The probe was deployed within the tumor with a diameter defined pre-operatively according to the size of the tumor. The probe was then maintained for seven minutes after the target temperature of 105°C was reached, as measured by the probe thermisters. For large tumors, the process was iterated with sequentially increasing diameters. After anatomical model extraction, we mimicked the RFA protocol by placing the virtual probe at the center of the tumor. Cells within a $3\,cm$-diameter (patient 2), or $4\,cm$ then $5\,cm$-diameter (patients 1 and 3) sphere around the probe tip were heated at 105°C during seven minutes for patient 2 or during two time seven minutes for patient 1 and 3. The simulation continued for three more minutes without the probe to reach

a steady state. Qualitatively, computed ablation followed closely the boundaries of the vessels, due to the heat sink effects of the blood. The shape of the ablated area also depended on the heat advection due to the small arteries (Fig. 4). Compared to postoperative images, temperature over the liver and cell death area computed using the model compared qualitatively well with the observed postoperative necrosis zone (Fig. 4, the lesion was manually segmented by an expert in postoperative CT images). Quantitatively, average point-to-mesh errors were $4.3 \pm 2.7\,mm$, $6.0 \pm 3.6\,mm$ and $11.9 \pm 5.2\,mm$. These errors were within clinical variability as they were lower than the different size configurations of the probes. More importantly, the simulation predicted that the selected protocols covered the entire lesion, which is the clinical criteria for ablation planning. Simulations took 8.30, 11.20 and $16.5\,min$ for patient 1, 2 and 3 respectively. To the best of our knowledge, this is the first time that real-time simulations of RFA ablation could be achieved. As one can see on (Fig. 4) patient 3 presented a large necrosis area compared to the ground truth, in this case the diffusion coefficient used from the literature was too high to get a perfect match.

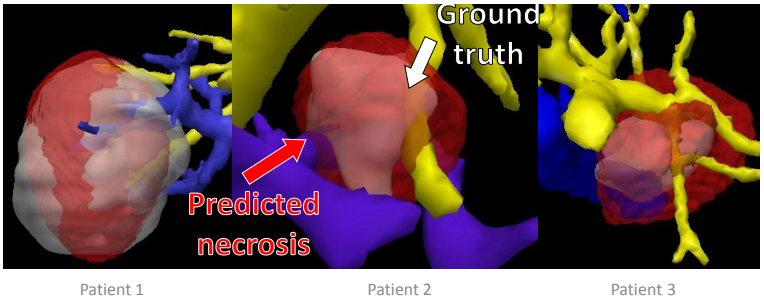

Fig. 4. Predicted necrosis compared qualitatively well with ground truth.

Table 1. Values of the parameters used in the simulation

parameter	description	value
ρ_b,ρ_t	blood and tissue densities	1.06×10^3 kg m^{-3}
c_b	blood heat capacity	4.18×10^3 J(kg K)$^{-1}$
c_t	tissue heat capacity	3.6×10^3 J(kg K)$^{-1}$
c_t*	tissue heat capacity in dead cells	0.67×10^3 J(kg K)$^{-1}$
d_b, d_t	blood and tissue heat conductivities	$0.512 \times (1+0.00161 \times (T-310))$ W(m K)$^{-1}$
H	convective transfer coefficient	24.4×10^4 W (m^3 K)$^{-1}$
ϵ	blood volume fraction	0.1
κ	permeability	4.0×10^{-11} m^2
μ	dynamic viscosity of the blood	$0.0035\,Pa\,s$
k_f	forward rate constant	3.33×10^{-3} s^{-1}
k_b	backward rate constant	7.77×10^{-3} s^{-1}
T_k	parameter of cell state model	40.5°C

4 Discussion and Conclusion

In this paper we have presented a first patient-specific model of liver tumor ablation that allows real-time computation. As we rely on Lattice-Boltzmann method, our framework does not require advanced meshing techniques and is applied directly from images using level set representation. We focused on modeling heat propagation and cell death based on a patient image taking into

account the heat sink effect of blood vessels and porous circulation in the liver. Despite possible biases in the manual registration of the postoperative images to the preoperative ones, and the use of biological parameters from the literature, which are not patient-specific, our model provided promising results, opening new opportunities in radio-frequency ablation planning and guidance. In this study we neglected the arterial flow. But it would be straightforward to include it for improved accuracy [14], provided the hepatic artery is visible in the image. Future works include validation on larger cohorts of patient, as well as coupling of blood flow and heat transfer models for more accurate predictions.

References

1. El-Serag, H.B., Davila, J.A., Petersen, N.J., McGlynn, K.A.: The continuing increase in the incidence of hepatocellular carcinoma in the united states: An update. Ann Intern Med **139** (2003) 817–823
2. Chen, X., Saidel, G.M.: Mathematical modeling of thermal ablation in tissue surrounding a large vessel. J Biomech **131** (2009)
3. Jiang, Y., Mulier, S., Chong, W., Diel Rambo, M., Chen, F., Marchal, G., Ni, Y.: Formulation of 3D finite elements for hepatic radiofrequency ablation. IJMIC **9** (2010) 225–235
4. Kröger, T., Pätz, T., Altrogge, I., Schenk, A., Lehmann, K., Frericks, B., Ritz, J., Peitgen, H., Preusser, T.: Fast estimation of the vascular cooling in RFA based on numerical simulation. Open biomed Eng J **4** (2010) 16
5. ONeill, D., Peng, T., Stiegler, P., Mayrhauser, U., Koestenbauer, S., Tscheliessnigg, K., Payne, S.: A three-state mathematical model of hyperthermic cell death. Ann Biomed Eng **39** (2011) 570–579
6. Yoshida, H., Nagaoka, M.: Multiple-relaxation-time lattice boltzmann model for the convection and anisotropic diffusion equation. Journal of Computational Physics **229** (2010) 7774 – 7795
7. Rapaka, S., Mansi, T., Georgescu, B., Pop, M., Wright, G., Kamen, A., Comaniciu, D.: LBM-EP: Lattice-boltzmann method for fast cardiac electrophysiology simulation from 3d images. In: MICCAI 2012. Volume 7511. (2012) 33–40
8. Pennes, H.H.: Analysis of tissue and arterial blood temperatures in the resting human forearm. J Appl Physiol **85** (1998) 5–34
9. Klinger, H.: Heat transfer in perfused biological tissue I: General theory. B Math Biol **36** (1974) 403 – 415
10. Grady: Random walks for image segmentation. Pattern Anal Mach Intell **28** (2006) 1768–1783
11. Nakayama, A., Kuwahara, F.: A general bioheat transfer model based on the theory of porous media. Int J Heat Mass Tran **51** (2008) 3190 – 3199
12. Yu, D., Mei, R., Luo, L.S., Shyy, W.: Viscous flow computations with the method of lattice boltzmann equation. Progress in Aerospace Sciences **39** (2003) 329 – 367
13. Ralovich, K., Itu, L., Mihalef, V., Sharma, P., Ionasec, R., Vitanovski, D., Krawtschuk, W., Everett, A., Ringel, R., Navab, N.: Hemodynamic assessment of pre-and post-operative aortic coarctation from MRI. MICCAI (2012) 486–493
14. Schenk Jr, W.G., McDonald, J.C., McDonald, K., Drapanas, T.: Direct measurement of hepatic blood flow in surgical patients: with related observations on hepatic flow dynamics in experimental animals. Ann Surg **156** (1962) 463